Hydrolysis Theory for Cisplatin and Its Analogues Based on Density Functional Studies

Yong Zhang,* Zijian Guo,* and Xiao-Zeng You

Contribution from the State Key Laboratory of Coordination Chemistry, Coordination Chemistry Institute, Nanjing University, Nanjing 210093, P. R. China

Received July 3, 2000

Abstract: Hydrolysis of cisplatin, the most widely used anticancer drug in the world, is believed to be the key activation step before the drug reaching its intracellular target DNA.To obtain an accurate hydrolysis theory for this important class of square-planar Pt(II) complexes, three typical reactions, i.e., the first and second hydrolyses of cisplatin and the hydrolysis of $[Pt(dien)Cl]^+$ (dien = diethylenetriamine), were studied at the experimental temperature with the solvent effect using mPW1PW91/SDD from a comprehensive methodological study on the Hartree−Fock (HF) ab initio method, electron correlation methods, pure density functional theory (DFT) methods, and hybrid HF-DFT methods with several basis sets. The true five stationary states in the second-order nucleophilic substitution (S_N2) pathway for the hydrolysis process, namely, reactant (R) → intermediate 1 (I1) → TS → intermediate 2 (I2) → product (P) were obtained and characterized theoretically for the first time. The most remarkable structural variations and the associated atomic charge variations in the hydrolysis process were found to occur in the equatorial plane of the five-coordinate trigonal-bipyramidal (TBP)-like structures of I1, TS, and I2. The reaction with the TS structure of smaller L−M−E angle and more lengthened M−L and M−E bonds was found to have a smaller Gibbs free energy change and accordingly the better hydrolysis yield. It is found that the sum of the three concentric angles in the TBP's equator is near 360° in I1 and I2 and is almost 360° in TS in each reaction. The associated energy profiles again demonstrated a typical S_N2 reaction curve. The computed forward and backward reaction enthalpy ($\Delta H^{\ddagger}$) and reaction entropy ($\Delta S^{\ddagger}$) in the rate-determining step I1 → TS → I2 are in good agreement with the experiments. Natural bonding orbital population analysis shows that the charge-separating extent follows the same order of ΔG in studied reactions. Comparing with the computational results of gas-phase reactions, it can be concluded that the solvent effect should be considered to obtain an accurate hydrolysis picture. The most affected structural parameters after solvation are related to the equatorial plane of the TBP-like geometry. The results provide theoretical guidance on detailed understanding on the mechanism of the hydrolysis of cisplatin, which could be useful in the design of novel Pt-based anticancer agents.

Introduction

With the vast development of computational chemistry in the past decade,[1] theoretical modeling of transition metal chemistry becomes much more mature than ever. The increasingly important role of computational transition metal chemistry in modern chemistry was demonstrated recently in a special issue of C*hemical Reviews* (**2000**, *100* (2)). Many important chemical and physical properties of the chemical systems can be predicted from first principles by various computational techniques.[1] In the fundamental fields of understanding mechanisms of reactions of transition metal complexes, it is generally accepted[2] that the density functional theory (DFT) methods give better and more reliable descriptions of the geometries and relative energies than traditional Hartree−Fock (HF) or Möller−Plesset perturbation theory at the second-order (MP2) methods except for some weak bonding interactions.[3] The DFT methods have actually been applied to a wide range of chemical reactions involving transition metal complexes, including not only the elementary reactions such as substitution, migratory insertion, hydrogen transfer, oxidative addition/reductive elimination, metathesis, and nucleophilic addition but also reactions concerning catalytic processes. The relativistic effective core potentials (RCEPs)[4−6] generated from the relativistic HF atomic core are especially valuable for heavy transition metal complexes due to the incorporation of the most important relativistic effect as well as the reduction of computational cost through the replacement of core electrons by means of pseudopotentials, which elevates the research efficiency on the other hand.

Platinum chemistry is one of the most extensive and versatile fields of chemistry,[7] because Pt can readily react with many organic and inorganic molecules to give rise to a rich class of interesting complexes. The finding of the anticancer activity of cisplatin,[8] the world best selling anticancer drug, has resulted in continuous interest in the kinetic studies of the hydrolysis of cisplatin and its analogues in various solution conditions,[9−16] which becomes a weighty part of contemporary medicinal

(1) *Reviews in Computational Chemistry*; Lipkowitz, K. B., Boyd, D. B., Eds.; VCH: New York, 1990−1999; Vols. 1−13.
(2) Niu, S.; Hall, M. B. *Chem. Rev.* **2000**, *100*, 353 and references therein.
(3) Cotton, F. A.; Feng, X.-J. *J. Am. Chem. Soc.* **1997**, *119*, 7514.
(4) Hay, P. J.; Wadt, W. R. *J. Chem. Phys.* **1985**, *82*, 299.
(5) Stevens, W.; Krauss, M.; Basch, H.; Jasien, P. G. *Can. J. Chem.* **1992**, *70*, 612.
(6) Leininger, T.; Nicklass, A.; Stoll, H.; Dolg, M.; Schwerdtfeger, P. *J. Chem. Phys.* **1996**, *105*, 1052 and previous papers by the same group.
(7) Dedieu, A. *Chem. Rev.* **2000**, *100*, 543 and references therein.
(8) Rosenberg, B.; Van Camp, L.; Trosko, J. E.; Mansour, V. H. *Nature* **1969**, *222*, 385.
(9) Tucker, M. A.; Colvin, C. B.; Martin, D. S. *Inorg. Chem.* **1964**, *3*, 1373.

10.1021/ja0023938 CCC: $20.00
Published on Web 08/28/2001

Scheme 1. Model Reactions Studied in This Work

Reaction 1: *cis*-$[PtCl_2(NH_3)_2] + H_2O \rightarrow$ *cis*-$[PtCl(OH_2)(NH_3)_2]^+ + Cl^-$

Reaction 2: *cis*-$[PtCl(OH_2)(NH_3)_2]^+ + H_2O \rightarrow$ *cis*-$[Pt(OH_2)_2(NH_3)_2]^{2+} + Cl^-$

Reaction 3: $[PtCl(dien)]^+ + H_2O \rightarrow [Pt(OH_2)(dien)]^{2+} + Cl^-$

inorganic chemistry.[17] Experimental studies of a variety of square-planar Pt(II) complexes[9,11,13,15] have shown that the rate constants for the first aquation step in acidic medium at 25 °C are of the same order of magnitude. For example, the first-step hydrolysis rate of cisplatin (see Scheme 1, reaction 1) in 1.0 M $HClO_4$ at 25 °C is 6.32×10^{-5} s^{-1}, which is merely slightly faster than that of the second step, 2.5×10^{-5} s^{-1}, under the same conditions (see Scheme 1, reaction 2).[15] This lack of variation of rate constants was recognized[10] as evidence for an associative mechanism in the aquation of Pt(II) system as well as other square-planar complexes.[12,18−19]

The direct theoretical efforts in elucidating these phenomena based on high-level quantum chemical investigations are, however, relatively more scarce than the experimental efforts. Some DFT and ab initio studies were concentrated on the molecular properties of cisplatin and its analogues.[20,21] Recent kinetic studies have shown that the substitutional ability and mechanism of transition metal complexes can be explained qualitatively in terms of the stability of the transition state or intermediate involved.[22−25] In an early ab initio MO study of the substitution reactions of square-planar transition metal complexes,[18] a five-coordinate trigonal-bipyramidal(TBP)-like transition state (TS) with a very small leaving ligand-to-metal-to-entering ligand angle in these systems was found and conformed by a recent DFT study.[19] This kind of TS structure is traced to minimize the repulsion between the d orbitals on the metal and the electron pairs on the entering and leaving ligands.[7] On the basis of a comparison of the activation energies, it was concluded that the associative mechanism was preferred to the dissociative mechanism in the main contribution to the substitution rates of these square-planar complexes.[19] A very recent work investigated the first hydrolysis process of cisplatin using a sophisticated molecular dynamics simulation.[26] With massive computational efforts, an activation enthalpy of ~24 kcal/mol was derived for the reaction.

For an accurate picture of the hydrolysis mechanisms of cisplatin and its analogues, the stationary points along the reaction pathway are essentially required from high-level quantum chemical optimizations and verified by the frequency analysis. The solvent effect, which was neglected in previous theoretical reaction studies,[18,19] should also be considered in these basic solution reactions to simulate the true experimental reaction process, especially in cases where the solvent effect is eminent. The capability of reproducing the correct order of kinetic and thermodynamic parameters in the class of the hydrolysis reactions for the square-planar cisplatin and its analogues is another important feature for an accurate candidate theory of the hydrolysis mechanisms, which is of fundamental importance in the understanding of the mechanism of reaction of the anticancer drug and in the design of novel agents. Dedicated to these aspects, this work was performed to build such an appropriate hydrolysis theory by employing advanced computational methods on three typical reactions in the class of title complexes as depicted in Scheme 1.

Theoretical Methods

Due to the cost-efficient procedure in the research of molecular properties, the density functional theory[27] itself has been developed rapidly and many DFT methods have been proposed and utilized in an ever-increasing number of theoretical investigations.[1,2,7,28−39] Generally, the functional can be separated into exchange and correlation parts. Several treatments can be used for the exchange part, such as Slater (S) or local spin density (LSD),[27,28] X_α,[27,28] Becke 88 (B),[29] Perdew−Wang 91 (PW91),[30] Barone's modified PW91 (mPW91),[31] and Gill 96 (G96).[32] The correlation part can also be considered through a variety of parametrizations such as VWN or LSD,[33] VWN5,[33] PL,[34] P86,[35] LYP,[36] PW91,[30] and B96.[37] With the inclusion of a mixture of HF exchange and DFT exchange−correlation, the hybrid HF-DFT treatments can be generated and have been proved to be more accurate than the pure DFT methods in describing various geometric and electronic properties of a broad range of chemical systems.[1−2,38,39] It has been shown[40−42] that many ground-state molecular properties produced by hybrid HF-DFT methods are remarkably accurate and even comparable to the CCSD(T) (coupled cluster calculations using both single and double substitutions from the Hartree−Fock determinant with the triple excitations noniteratively included) results. These advantageous features have enabled the hybrid HF-DFT methods to become the dominant computational tools for the treatment

(10) Benson, D. *Mechanisms of Inorganic Reactions in Solution*; McGraw-Hill: London, 1968.
(11) Roley, R.; Martin, D. S. *Inorg. Chim. Acta* **1973**, *7*, 573.
(12) (a) Jestin, J.-L.; Chottard, J.-C.; Frey, U.; Layrenczy, G.; Merbach, A. E. *Inorg. Chem.* **1994**, *33*, 4277. (b) Mikola, M.; Klika, K. D.; Hakala, A.; Arpalahti, J. *Inorg. Chem.* **1999**, *38*, 571.
(13) (a) Miller, S. E.; House, D. A. *Inorg. Chim. Acta* **1989**, *161*, 131. (b) Miller, S. E.; House, D. A. *Inorg. Chim. Acta* **1989**, *166*, 189.
(14) Miller, S. E.; House, D. A. *Inorg. Chim. Acta* **1990**, *173*, 53.
(15) Miller, S. E.; House, D. A. *Inorg. Chim. Acta* **1991**, *187*, 125.
(16) (a) Basolo, F.; Gray, H. B.; Pearson, R. G. *J. Am. Chem. Soc*. **1960**, *82*, 4200. (b) Marti, N.; Hoa, G. H. B. B.; Kozelka, J. *Inorg. Chem. Commun.* **1998**, *1*, 439.
(17) (a) Wong, E.; Giandomenico, C. M. *Chem. Rev.* **1999**, *99*, 2451. (b) Jamieson, E. R.; Lippard, S. J. *Chem. Rev*. **1999**, *99*, 2467. (c) Reedjik, J. *Chem. Rev*. **1999**, *99*, 2499.
(18) Lin, Z.; Hall, M. B. *Inorg. Chem.* **1991**, *30*, 646.
(19) Deeth, R. J.; Elding, L. I. *Inorg. Chem.* **1996**, *35*, 5019.
(20) (a) Carloni, P.; Andreoni, W.; Hutter J.; Curioni, A.; Giannozzi, P.; Parrinello, M. *Chem. Phys. Lett.* **1995**, *234*, 50. (b) Tornaghi, S.; Andreoni, W.; Carloni, P.; Hutter J.; Parrinello, M. *Chem. Phys. Lett.* **1995**, *246*, 469.
(21) Pavankumar, P. N. V.; Seetharamulu, P.; Yao, S.; Saxe, J. D.; Reddy, D. G.; Hausheer, F. H. *J. Comput. Chem.* **1999**, *20*, 365.
(22) Basolo, F. *Inorg. Chim. Acta* **1985**, *100*, 3.
(23) Basolo, F. *Polyhedron* **1990**, *9*, 1503.
(24) Basolo, F. *Pure Appl. Chem.* **1988**, *60*, 1193.
(25) Herrington, T. R.; Brown, T. L. J. *J. Am. Chem. Soc.* **1985**, *107*, 5700.
(26) Carloni, P.; Sprik, M.; Andreoni, W. *J. Phys. Chem. B* **2000**, *104*, 823.
(27) Hohenberg, P.; Kohn, W. *Phys. Rev. B* **1964**, *136*, 864.
(28) Slater, J. C. In *Quantum Theory of Molecules and Solids*, Vol. 4: *The Self-Consistent Field for Molecules and Solids*; McGraw-Hill: New York, 1974.
(29) Becke, A. D. *Phys. Rev. A* **1988**, *38*, 3098.
(30) Perdew, J. P.; Burke, K.; Wang, Y. *Phys. Rev. B* **1996**, *54*, 16533.
(31) Adamo, C.; Barone, V. *J. Chem. Phys.* **1998**, *108*, 664.
(32) Gill, P. M. W. *Mol. Phys.* **1996**, *89*, 433.
(33) Vosko, S. H.; Wilk, L.; Nusair, M. *Can. J. Phys.* **1980**, *58*, 1200.
(34) Perdew, J. P.; Zunger, A. *Phys. Rev.* B **1981**, *23*, 5048.
(35) Perdew, J. P. *Phys. Rev. B* **1986**, *33*, 8822.
(36) Lee, C.; Yang, W.; Parr, R. G. *Phys. Rev. B* **1988**, *37*, 785.
(37) Becke, A. D. *J. Chem. Phys.* **1996**, *104*, 1040.
(38) Ruiz, E.; Salahub, D. R.; Vela, A. *J. Am. Chem. Soc.* **1995**, *117*, 1141.
(39) Zhang, Y.; Zhao, C.-Y.; You, X.-Z. *J. Phys. Chem. A* **1997**, *101*, 2879.
(40) Gill, P. M. W.; Johnson, B. G.; Pople, J. A. *Chem. Phys. Lett*. **1992**, *197*, 499.
(41) Scuseria, G. E. *J. Chem. Phys.* **1992**, *97*, 7528.
(42) Oliphant, N.; Bartlett, R. J. *J. Chem. Phys*. **1994**, *100*, 6550.

of transition metal reactions.[2,7] In the quantum chemical software package Gaussian 98[43] employed here, there are several kinds of hybrid HF-DFT treatments available. In addition to the widely used Becke's three-parameter functionals[44] B3LYP, B3PW91, and B3P86 and the BH and HLYP functional (B is the Becke treatment[29] of the exchange functional, HandH means half Hartree−Fock exchange and half Slater exchange, and LYP stands for the Lee−Yang−Parr parametrizations[36] of the correlation functional), there are some recently proposed functionals, such as Becke's one-parameter functional[37,45] B1LYP using the LYP correlation functional[36] and Barone and Adamo's Becke-style one-parameter functional [31] mPW1PW91 using modified PW exchange and PW91 correlation.[30]

Among available ECP basis sets, the commonly used ones were formulated as LanL,[4] CEP,[5] and SDD.[6] They differ in the schemes of fitting the ECP to Gaussian functions. The way of treating light atoms and valence electrons is also varied in these three basis sets. First-row atoms are treated with all-electron basis sets of Dunning/Huzinaga full double-ζ (D95)[46] and Dunning/Huzinaga valence double-ζ (D95V)[46] and ECP basis sets for LanL, SDD, and CEP, respectively. In Gaussian 98,[43] there are one SDD basis set, two LanL basis sets (LanL2DZ, LanL2MB), and three CEP basis sets (CEP-4G, CEP-31G, CEP-121G). The difference between LanL2DZ and LanL2MB lies in the treatment of first-row atoms, where the minimum basis set STO-3G other than D95 is employed for LanL2MB. So LanL2DZ is more widely used than LanL2MB. The difference among three CEP basis sets lies in the contraction scheme:[5] CEP-4G, CEP-31G, and CEP-121G are the Stevens/Basch/Krauss ECP minimal basis set, split valence basis set, and triple-split basis set, respectively. As a matter of fact, there is only one CEP basis set defined beyond the second row in Gaussian 98,[43] and all three keywords are equivalent for these atoms. The sizes of these basis sets are in the sequence of SDD > CEP-121G > LanL2DZ. For example, the numbers of basis functions for cisplatin are 68, 100, and 107 with LanL2DZ, CEP-121G, and SDD basis sets, respectively.

Since a proper structure is a primary condition for in-depth studies of a chemical system, it is necessary to select an appropriate computational model that can reproduce the reasonable structures for title complexes. For this purpose, we first compared the effects of different computational models on the optimization of molecular structures of some studied compounds (vide infra). Then, with the selected computational model, all the relevant species in the three hydrolysis reactions including the chlorine anion, the water molecule, and other 14 complexes (see Chart 1) were fully optimized in both gas phase and aqueous solution. Subsequent frequency analyses were taken to verify the nature of these stationary states in their potential energy surfaces, i.e., all positive frequencies and eigenvalues ensuring a minimal state, and one imaginary frequency and one negative eigenvalue ensuring a transition state. Thermal contributions to the energetic properties were also considered at the standard state, namely, at 298.15 K and 1 atm. In all these computations, the default techniques and criteria of the self-consistent-field (SCF) calculations, geometry optimizations, and frequency calculations in Gaussian 98[43] were adopted.

To incorporate the solvent effect, a family of the self-consistent reaction field (SCRF) methods[47−54] has been devised for computing systems in aqueous or nonaqueous solutions, such as the Onsager model,[47−51] the polarized continuum (overlapping spheres) model (PCM),[52−59] the (static) isodensity surface polarized continuum model (IPCM),[60] and the self-consistent isodensity PCM (SCI−PCM) model.[60] In these SCRF models, the solvent is taken as a continuum of uniform dielectric constant ϵ—the reaction field, where the solute is placed in a cavity within the solvent. The difference in these SCRF models rests in the way they define the cavity and the reaction field. Among all these SCRF models, the Onsager reaction field model[47,48] is a classic one and has been adapted to various kinds of solution calculations[49−51] though it may not yield solvation parameters to high precision. In this method, the solute occupies a fixed spherical cavity of radius a_0 within the solvent field. A dipole in the molecule will induce a dipole in the medium, and the electric field applied by the solvent dipole will in turn interact with the molecular dipole, leading to the net stabilization. Due to its modest computational cost and relative accuracy and also a computational problem of another solution optimization model, SCIPCM in Gaussian 98[43] for title complexes, the Onsager SCRF model was utilized in this work to optimize the solvated systems and calculate relevant properties of title aqueous reactions. The cavity size, a_0, for each solvated species was derived from a tight molecular volume calculation provided in Gaussian 98[43] on the fully optimized gas-phase stationary states using the same quantum chemical model for consistency.

Results and Discussion

1. Effects of Different Computational Models on the Optimizations of Molecular Structures. To illustrate the effects of different computational models on structures, we have carried out a broad range of quantum chemical calculations on water (a component in title reactions), $PtCl_4^{2-}$ (a small platinum-containing species), and cisplatin. Detailed discussion on the computational methods is provided in the Supporting Information. As shown in Tables 1 and 2, gradient-corrected DFT methods exaggerate the metal−ligand bond length and different models have little effect. It is the most recently developed

(43) Gaussian 98, Revision A.7. Frisch, M. J.; Trucks, G. W.; Schlegel, H. B.; Scuseria, G. E.; Robb, M. A.; Cheeseman, J. R.; Zakrzewski, V. G.; Montgomery, Jr., J. A.; Stratmann, R. E.; Burant, J. C.; Dapprich, S.; Millam, J. M.; Daniels, A. D.; Kudin, K. N.; Strain, M. C.; Farkas, O.; Tomasi, J.; Barone, V.; Cossi, M.; Cammi, R.; Mennucci, B.; Pomelli, C.; Adamo, C.; Clifford, S.; Ochterski, J.; Petersson, G. A.; Ayala, P. Y.; Cui, Q.; Morokuma, K.; Malick, D. K.; Rabuck, A. D.; Raghavachari, K.; Foresman, J. B.; Cioslowski, J.; Ortiz, J. V.; Baboul, A. G.; Stefanov, B. B.; Liu, G.; Liashenko, A.; Piskorz, P.; Komaromi, I.; Gomperts, R.; Martin, R. L.; Fox, D. J.; Keith, T.; Al-Laham, M. A.; Peng, C. Y.; Nanayakkara, A.; Gonzalez, C.; Challacombe, M.; Gill, P. M. W.; Johnson, B.; Chen, W.; Wong, M. W.; Andres, J. L.; Gonzalez, C.; Head-Gordon, M.; Replogle, E. S.; Pople, J. A.; Gaussian, Inc., Pittsburgh, PA, 1998.

(44) Becke, A. D. *J. Chem. Phys.* **1993**, *98*, 5648.

(45) Adamo, C.; Barone, V. *Chem. Phys. Lett.* **1997**, *274*, 242.

(46) Dunning Jr., T. H.; Hay, P. J. In *Modern Theoretical Chemistry*; Schaefer, H. F., III, Ed.; Plenum: New York, 1976; Vol. 3.

(47) Kirkwood, J. G. *J. Chem. Phys.* **1934**, *2*, 351.

(48) Onsager, L. *J. Am. Chem. Soc.* **1936**, *58*, 1486.

(49) Wong, M. W.; Frisch, M. J.; Wiberg, K. B. *J. Am. Chem. Soc.* **1991**, *113*, 4776.

(50) Wong, M. W.; Wiberg, K. B.; Frisch, M. J. *J. Am. Chem. Soc.* **1992**, *114*, 523.

(51) Wong, M. W.; Wiberg, K. B.; Frisch, M. J. *J. Am. Chem. Soc.* **1992**, *114*, 1645.

(52) Miertus, S.; Scrocco, E.; Tomasi, J. *Chem. Phys.* **1981**, *55*, 117.

(53) Miertus, S.; Tomasi, J. *Chem. Phys.* **1982**, *65*, 239.

(54) Cossi, M.; Barone, V.; Cammi, R.; Tomasi, J. *Chem. Phys. Lett.* **1996**, *255*, 327.

(55) Cances, M. T.; Mennucci, V.; Tomasi, J. *J. Chem. Phys.* **1997**, *107*, 3032.

(56) Barone, V.; Cossi, M.; Mennucci, B.; Tomasi, J. *J. Chem. Phys.* **1997**, *107*, 3210.

(57) Cossi, M.; Barone, V.; Mennucci, B.; Tomasi, J. *Chem. Phys. Lett.* **1998**, *286*, 253.

(58) Barone, V.; Cossi, M.; Tomasi, J. *J. Comput. Chem.* **1998**, *19*, 404.

(59) Barone, V.; Cossi, M. *J. Phys. Chem. A* **1998**, *102*, 1995.

(60) Foresman, J. B.; Keith, T. A.; Wiberg, K. B.; Snoonian, J.; Frisch, M. J. *J. Phys. Chem.* **1996**, *100*, 16098.

Chart 1. Molecular Configurations of the Studied Complexes

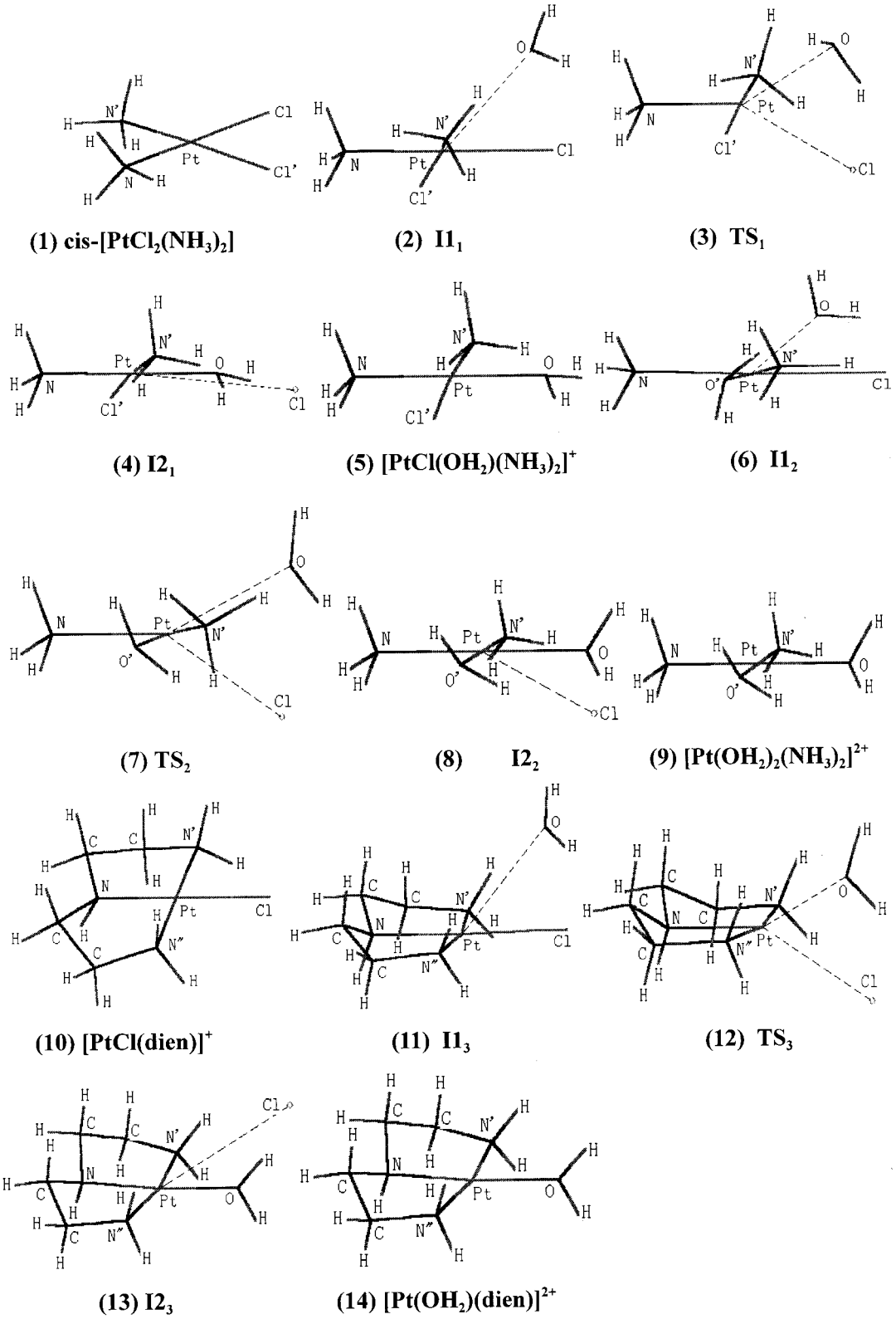

mPW1PW91 functional[31] that predicts the gas-phase cisplatin structure most approximate to the experimental crystal structure.[61] The performance of the employed basis sets was found to generally follow the same order of their size, namely, SDD > CEP-121G = CEP-31G > LanL2DZ. It should be noted that none of these methods can produce bond angles of the same quality as for bond lengths. This methodological study suggests that further amelioration of the accuracy of predicting these complexes' structures may possess great dependence on the improvement of the pseudopotential basis set, which has been validated by the recent comprehensive ab initio quantum chemical studies using pure ECP and hybrid HF/ECP basis sets.[21]

The mPW1PW91/SDD geometry for another title complex, $[PtCl(dien)]^+$, is even better than for cisplatin as compared to the X-ray crystal structure.[62] Therefore, the mPW1PW91/SDD

(61) Milburn, G. H. W.; Truter, M. R. *J. Chem. Soc. A* **1966**, 1609.

Table 1. Methodological Study on H_2O and $PtCl_4^{2-}$

method	H_2O (Å, deg)	method	$PtCl_4^{2-}$ (Å)
expt[a]	0.958, 104.51	expt[b]	2.34
BLYP/SDD	0.989, 108.62	mPW1PW91/SDD	2.422
B3LYP/SDD	0.977, 110.04	BHandHLYP/SDD	2.436
B3PW91/SDD	0.974, 110.27	B3LYP/SDD	2.455
B3P86/SDD	0.974, 110.38		
B1LYP/SDD	0.975, 110.30		
MPW1PW91/SDD	0.971, 110.44		
BHandHLYP/SDD	0.963, 111.41		
MP2/SDD	0.979, 110.64		
CCSD(T)/SDD	0.980, 110.28		
mPW1PW91/CEP-121G	0.971, 110.32	mPW1PW91/CEP-121G	2.429
BHandHLYP/CEP-121G	0.963, 111.07	BHandHLYP/CEP-121G	2.441
		mPW1PW91/CEP-31G	2.429
		BHandHLYP/CEP-31G	2.441
		mPW1PW91/LanL2DZ	2.442
		BHandHLYP/LanL2DZ	2.453

[a] Reference 63. The structural parameters are O−H bond length and ∠H−O−H bond angle. [b] Reference 64. The structural parameter is Pt−Cl bond length.

Table 2. Methodological Comparisons on the Molecular Structure of Cisplatin

method	R_{Pt-Cl} (Å)	R_{Pt-N} (Å)	∠Cl−Pt−Cl (deg)	∠N−Pt−N (deg)
expt[a]	2.33 ±0.01	2.01 ±0.04	91.9 ±0.3	87 ±1.5
other[b])	2.315	2.065	95.5	98.0
HF/Lanl2DZ	2.415	2.126	97.1	95.7
MP2/Lanl2DZ	2.405	2.123	95.9	97.5
S/Lanl2DZ	2.403	2.076	96.9	101.0
$X_{\alpha/Lanl2DZ}$	2.381	2.056	96.8	100.9
B/Lanl2DZ	2.485	2.187	96.9	99.4
BPL/Lanl2DZ	2.452	2.155	96.9	99.5
BVWN/Lanl2DZ	2.447	2.150	96.8	99.6
BVWN5/Lanl2DZ	2.451	2.154	96.8	99.5
BLYP/Lanl2DZ	2.435	2.129	97.0	100.2
BP86/Lanl2DZ	2.410	2.100	96.8	100.4
BPW91/Lanl2DZ	2.410	2.102	96.6	100.3
B3LYP/Lanl2DZ	2.411	2.111	96.7	99.3
B1LYP/Lanl2DZ	2.411	2.113	96.7	99.0
B3PW91/Lanl2DZ	2.393	2.091	96.3	99.3
B3P86/Lanl2DZ	2.388	2.085	96.4	99.5
BHandHLYP/Lanl2DZ	2.393	2.099	96.6	98.0
mPW1PW91/Lanl2DZ	2.386	2.086	96.2	99.2
B/SDD	2.470	2.189	96.4	98.6
MP2/SDD	2.375	2.097	95.9	97.5
B3LYP/SDD	2.393	2.109	96.2	98.6
B1LYP/SDD	2.394	2.111	96.2	98.4
BHandHLYP/SDD	2.377	2.098	96.1	97.5
mPW1PW91/SDD	2.368	2.084	95.9	98.6

[a] Reference 61. [b] Reference 20.

model was employed for all the geometry optimizations, single-point energy calculations, and frequency analyses of both gas-phase and subsequent solution-phase systems studied here.

With the selected mPW1PW91/SDD model, values of cavity sizes (a_0) for the chlorine anion, the water molecule, and complexes **1**−**14** (see Chart 1) recommended by the tight molecular volume calculations on the fully optimized gas-phase stationary states were 2.80, 2.54, 4.25, 4.29, 4.25, 4.27, 4.02, 4.17, 4.30, 4.24, 3.71, 4.49, 4.52, 4.57, 4.50, and 4.42 Å, respectively.

2. Geometry Profiles of Hydrolysis Reactions of Cisplatin and Its Analogues in Aqueous Solution. The hydrolysis reactions of the title complexes are characterized by an exchange of two ligands, the chlorine anion and the water molecule, which belong to the class of second-order nucleophilic substitution (S_N2) reactions.[65] These reactions proceed via a collision between the reactants, with the nucleophilic species—H_2O or OH^- in the basic pH conditions—attacking the metal center to release the ionic ligand, Cl^-. In such a process, a transition structure in which the entering ligand, the leaving ligand, and the metal complex being weakly bound can be found.[18−19,22−25] In a general S_N2 reaction pathway, five stationary states, i.e., reactant (R) → intermediate 1 (I1) → TS → intermediate 2 (I2) → product (P), are present.[65] It was the first time to directly obtain these stationary states for the hydrolysis reactions of the title complexes on the basis of the theoretical optimization and subsequent frequency validation. Specifically, the R, I1, TS, I2, and P relevant to model reactions 1, 2, and 3 are designated by the subscripts 1, 2, and 3, respectively. As seen in Chart 1, the five-coordinate TBP-like transition states are complexes **3**, **7**, and **12** for model reactions 1, 2, and 3, respectively. The associated intermediates, complexes **2** and **4**, **6** and **8**, and **11** and **13** for model reactions 1, 2, and 3, respectively, were all found to be five-coordinate. The similarity of the structures of the transition and intermediate states in title reactions and in other substitution reactions of square-planar transition metal complexes[18,19] suggests that the associative mechanism may be preferred according to others' theoretical comparisons.[19] Such preferences for the associative mechanism and the five-coordinate TS structure were consistent with the experimental studies on the aquation of some substituted Pt(II) complexes with different in vivo anticancer activities.[12] The common five-coordinate structural topology for TS, I1, and I2 was illustrated in Chart 2. The structural variations of some typical bond lengths and bond angles associated with the hydrolysis process are listed in Table 3 for model reactions 1, 2**,** and 3.

In TS structures of some substitution reactions of square-planar transition metal complexes,[18,19] the leaving ligand-to-metal-to-entering ligand (L−M−E) angle was reported to be smaller than 90°, indicating a high steric effect.[18] The hydrolysis reactions of cisplatin and its analogues studied here showed that their L−M−E angles (namely, ∠Cl−Pt−O) are even smaller. As shown in Table 3, the metal-to-leaving ligand (M−L) bond

(62) Britten, J. F.; Lock, C. J. L.; Pratt, W. M. C. *Acta Crystallogr. B* **1982**, *38*, 2148.

(63) *CRC Handbook of Chemistry and Physics*, 78th ed.; Lide, D. R., Ed.; CRC Press: Boca Raton, FL, 1992.

(64) Atoji, M.; Ritchardson, J. W.; Rundle, R. E. *J. Am. Chem. Soc.* **1957**, *79*, 3017.

(65) Shi, Z.; Boyd, R. J. *J. Am. Chem. Soc.* **1989**, *111*, 1575.

Chart 2. Common Structure for the Characterization of Geometric Parameters of the Reactants, Intermediates, Transition States, and Products[a]

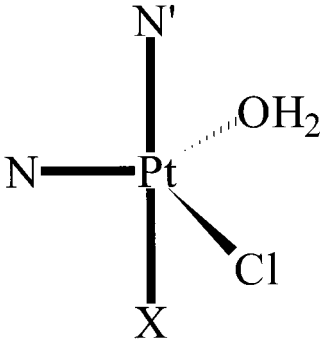

[a] X Is Cl′, O′, and N″, respectively, in the first and second hydrolysis of cisplatin and hydrolysis of $[PtCl(dien)]^+$.

length (R_{Pt-Cl}) and the metal-to-entering ligand (M−E) bond length (R_{Pt-O}) in the TS are more lengthened respectively than in the reactant and product structures. These characteristically small L−M−E angles and the corresponding long metal−ligand bonds can efficiently minimize the repulsion between the d orbitals on the metal and the electron pairs on the entering and leaving ligands.[7,18,19] Compared with the TS structures, the L−M−E angles in the associated intermediates are further reduced, which effectively contribute to decreasing electronic repulsion between metal and ligands.

It can be seen from Table 3 that, based on the current DFT studies, the most remarkable structural variations in the hydrolysis process occur in the M−L bond length (R_{Pt-Cl}), M−E bond length (R_{Pt-O}), the L−M−E bond angle (∠Cl−Pt−O), the leaving ligand to metal to the resting equatorial ligand (L−M−R) bond angle (∠Cl−Pt−N), and the entering ligand to metal to the resting equatorial ligand (E−M−R) bond angle (∠O−Pt−N). This phenomenon implies that the geometric changes associated with the hydrolysis mainly take place in the equatorial plane of the TBP-like structure. Actually, even the smallest structural change in the equatorial plane, namely, the variation of the metal to the resting equatorial ligand bond length (R_{Pt-N}) is ∼2 times that of the changes in the other two bond lengths of the TBP-like structure, as shown in Table S1 (Supporting Information). As clearly depicted in Figures 1 and 2, R_{M-L} increases more with the hydrolysis process, while R_{M-E} decreases less. The changes of bond lengths and bond angles are concordant with their reaction nature as the ligand replacement. Although variations of the L−M−E, L−M−R, and E−M−R angles alone can be as large as ∼60° in some cases (see Figure 2), it is interesting to point out that their summation (∑ in Table 3) shifts only in a narrow band of less than 9°. In particular, this value of TS is almost 360° for each reaction in both the gas phase and the aqueous solution, indicating a coplanar position of N, Pt, O, and Cl in the TS, though the previous methodological study shows that the current computational model cannot produce bond angles of the same quality as for bond lengths. Therefore, the equator geometry of the five-coordinate TBP-like structure significantly affects the hydrolyses of cisplatin and its analogues.

The rather similar structures and structural variation tendencies of the five stationary states, i.e., R, I1, TS, I2, and P, for three studied model reactions indicate that a common mechanism for the hydrolyses of cisplatin and its analogues is acceptable, which builds the theoretical ground for the present effort for this class of reactions.

Table 3. Key Geometrical Parameters of Platinum-Containing Species in the Hydrolyses[a]

rxn	parameter	phase	R	I1	TS	I2	P
1	R_{Pt-Cl} (Å)	gas	2.368	2.383	2.742	3.953	
		sol	2.390	2.399	2.819	4.135	
		Δ	0.022	0.016	0.077	0.182	
	R_{Pt-O} (Å)	gas		3.610	2.401	2.030	2.087
		sol		3.667	2.420	2.042	2.077
		Δ		0.057	0.019	0.012	−0.010
	∠Cl−Pt−O	gas		58.0	68.3	43.8	
	(deg)	sol		58.7	66.7	39.5	
		Δ		0.7	−1.6	−4.3	
	∠Cl−Pt−N	gas	178.6	177.7	143.4	139.7	
	(deg)	sol	180.0	178.3	146.4	145.7	
		Δ	1.4	0.6	3.0	6.0	
	∠O−Pt−N	gas		123.8	148.3	176.3	176.1
	(deg)	sol		121.6	146.9	174.7	179.4
		Δ		−2.2	−1.4	−1.6	3.3
	∑ (deg)	gas		359.5	360.0	359.8	
		sol		358.5	360.0	360.0	
		Δ		−1.0	0.0	0.2	
2	R_{Pt-Cl} (Å)	gas	2.344	2.366	2.710	3.527	
		sol	2.385	2.401	2.792	4.095	
		Δ	0.041	0.035	0.082	0.568	
	R_{Pt-O} (Å)	gas		3.566	2.343	2.053	2.082
		sol		3.551	2.444	2.079	2.083
		Δ		−0.015	0.101	0.026	0.001
	∠Cl−Pt−O	gas		60.5	68.7	53.6	
2	(deg)	sol		59.9	66.8	44.5	
		Δ		−0.6	−1.9	−9.1	
	∠Cl−Pt−N	gas	176.7	176.2	133.7	121.4	
	(deg)	sol	178.5	176.6	143.6	133.7	
		Δ	1.8	0.4	9.9	12.3	
	∠O−Pt−N	gas	/	115.7	157.5	174.8	179.1
	(deg)	sol		116.8	149.4	178.1	179.1
		Δ		1.1	−8.1	3.3	0.0
	∑ (deg)	gas		352.4	359.9	349.8	
		sol		353.3	359.8	356.3	
		Δ		0.9	−0.1	6.5	
3	R_{Pt-Cl} (Å)	gas	2.347	2.367	2.695	3.400	
		sol	2.378	2.397	2.783	4.018	
		Δ	0.031	0.030	0.088	0.618	
	R_{Pt-O} (Å)	gas		3.531	2.305	2.057	2.099
		sol		3.548	2.363	2.072	2.093
		Δ		0.017	0.058	0.015	−0.006
	∠Cl−Pt−O	gas		62.1	69.1	56.1	
	(deg)	sol		61.2	67.1	44.0	
		Δ		−0.9	−2.0	−12.1	
	∠Cl−Pt−N	gas	178.7	176.9	133.9	117.9	
	(deg)	sol	179.1	177.4	141.7	132.1	
		Δ	0.4	0.5	7.8	14.2	
	∠O−Pt−N	gas		116.4	156.7	172.1	179.9
	(deg)	sol		117.1	151.2	175.5	179.9
		Δ		0.7	−5.5	3.4	0.0
	∑ (deg)	gas		355.4	359.7	346.1	
		sol		355.7	360.0	351.6	
		Δ	/	0.3	0.3	5.5	/

[a] Phase gas and sol are gas phase and aqueous solution, respectively. Phase Δ is the solvent effect defined as the property in the aqueous solution minus that in gas phase. ∑ is the sum of ∠O−Pt−N, ∠Cl−Pt−N, and ∠O−Pt−Cl. Please see Chart 1 for the definition of the structure concerned.

3. Thermodynamic Profiles of Hydrolysis Reactions of Cisplatin and Its Analogues in Aqueous Solution. To quantitatively assess the hydrolysis behaviors based on the electronic properties, various kinds of energetic terms were computed with the incorporation of thermal effects at 298.15 K for comparison with experiments carried out at this temperature. These properties are listed in Table S2 (Supporting Information). The present work, which is based on the analyses of the true R−I1−TS−I2−P stepwise hydrolysis process, shows that not only the reaction in gas phase but also the reaction in aqueous solution with different ligands undergoes the same S_N2

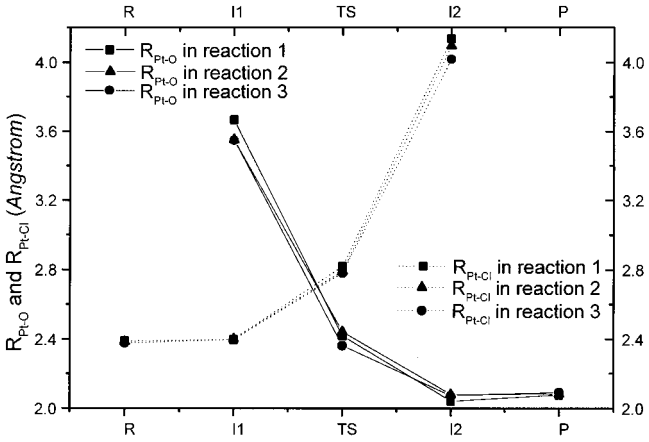

Figure 1. Bond length variation of Pt−O and Pt−Cl (see Chart 2 for their definitions) during the hydrolysis in aqueous solution for the five states (R, I1, TS, I2, P) in the three model reactions. These states were connected by straight lines for clarity of the illustration.

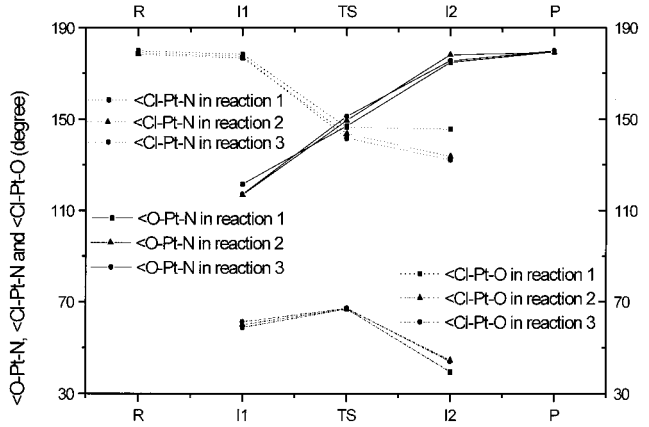

Figure 2. Bond angle variation of ∠O−Pt−N, ∠Cl−Pt−N, and ∠Cl−Pt−O (see Chart 2 for their definitions) during the hydrolysis in aqueous solution for the five states (R, I1, TS, I2, P) in the three model reactions. These states were connected by straight lines for clarity of the illustration.

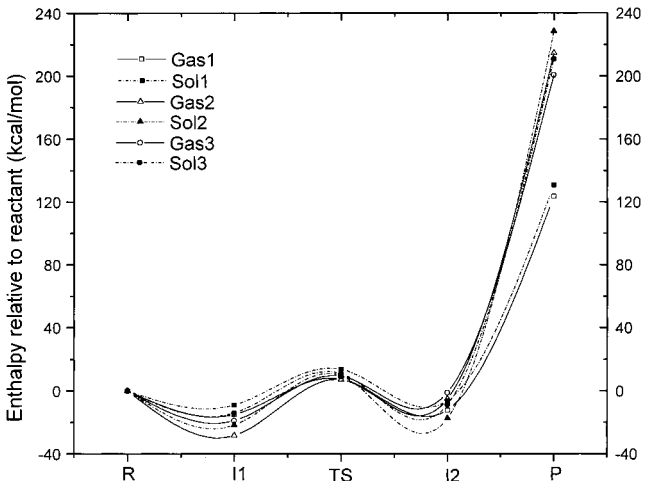

Figure 3. SN_2 reaction map of the calculated enthalpies for the five states (R, I1, TS, I2, P) with respect to R in each model reaction. These states were connected by spline lines for clarity of the illustration. The symbols of Gas and Sol in this figure represent gas-phase reaction and aqueous solution reaction, respectively.

mechanism. It can be seen from Figure 3 that, in each model reaction in both gas phase and aqueous solution, the reactant drops down to form the more energetically favorable intermediate I1, then climbs uphill to TS, which afterward lowers its energy to produce the second intermediate I2, and finally gives rise to the hydrolysis product. This curve has that general shape of the S_N2 reaction.[65]

Table 4. Theoretical Results of the Studied Hydrolysis Reactions[a]

hydrolysis	step	phase	*S* (cal/mol·K)	*H* (kcal/mol)	*G* (kcal/mol)
1	$R_1 \rightarrow P_1$	gas	−8.42	123.50	126.01
		sol	−8.28	130.69	133.15
		Δ	0.14	7.19	7.14
	$I1_1 \rightarrow I2_1$	gas	−2.71	2.77	3.58
		sol	−3.18	2.77	3.72
		Δ	−0.47	0.00	0.14
	$I1_1 \rightarrow TS_1$	gas	−3.90	22.46	23.63
		sol	−4.36	22.81	24.11
		Δ	−0.46	0.35	0.48
	$I2_1 \rightarrow TS_1$	gas	−1.19	19.69	20.05
		sol	−1.18	20.04	20.39
		Δ	0.01	0.35	0.34
2	$R_2 \rightarrow P_2$	gas	−10.67	214.37	217.55
		sol	−11.34	228.29	231.66
		Δ	−0.67	13.92	14.11
	$I1_2 \rightarrow I2_2$	gas	−2.66	23.28	24.08
		sol	−1.17	4.15	3.80
		Δ	1.49	−19.13	−20.28
	$I1_2 \rightarrow TS_2$	gas	−3.96	35.39	36.57
		sol	−3.43	31.24	32.27
		Δ	0.53	−4.15	−4.30
	$I2_2 \rightarrow TS_2$	gas	−1.30	12.11	12.49
		sol	−2.26	27.09	28.47
		Δ	−0.96	14.98	15.98
3	$R_3 \rightarrow P_3$	gas	−9.24	198.32	203.35
		sol	−9.62	208.59	213.60
		Δ	−0.38	10.27	10.25
	$I1_3 \rightarrow I2_3$	gas	−4.29	17.84	18.83
		sol	−6.56	5.43	5.79
		Δ	−2.27	−12.41	−13.04
	$I1_3 \rightarrow TS_3$	gas	−4.12	28.20	29.43
		sol	−3.73	24.88	25.99
		Δ	0.39	−3.32	−3.44
	$I2_3 \rightarrow TS_3$	gas	−8.41	10.36	10.60
		sol	−10.29	19.45	20.20
		Δ	−1.88	9.09	9.60

[a] Phase gas and sol are gas phase and aqueous solution, respectively. Phase Δ is the solvent effect defined as the property in the aqueous solution minus that in gas phase.

Due to the nature of the S_N2 mechanism in these hydrolysis reactions, the rate-determining step is from the first intermediate toward the second intermediate via the transition state (step I1 → I2 in Table 4). So the enthalpy change in this step is the reaction barrier $\Delta H^{\ddagger}$. It can be seen from Table 4 that the forward and backward $\Delta H^{\ddagger}$ derived from the current DFT solution calculations are 22.81 and 20.04 kcal/mol, respectively, for reaction 1**,** which are close to the experimental data[15] of 19.67 and 17.87 kcal/mol, respectively. The recent elaborate quantum molecular dynamics simulation on this reaction[26] obtained a similar reaction barrier (∼24 kcal/mol) despite its massive computational efforts. The computational $\Delta S^{\ddagger}$ is somewhat smaller than the experimental value[15] but has the same sign.

As shown in Table 4, the ΔG data of these three step reactions are 3.72, 3.80, and 5.79 kcal/mol in model hydrolysis reactions 1, 2, and 3, respectively. This result conforms to the experimental fact[15,16] that $K_1 > K_2 \gg K_3$ (K_1, K_2, and K_3 are equilibrium constants of reactions 1, 2, and 3, respectively), since $\Delta G = -RT \ln K$.

To get more electronic information for these hydrolysis reactions, the natural bonding orbital (NBO)[66] charges were

Table 5. Natural Bonding Orbital Populations in Studied Hydrolysis Reactions[a]

hydrolysis	atom	phase	R	I1	TS	I2	P
1	Pt	gas	0.490	0.503	0.646	0.634	0.612
		sol	0.522	0.530	0.663	0.634	0.642
		Δ	0.032	0.027	0.017	0.000	0.030
	Cl	gas	−0.492	−0.507	−0.686	−0.686	−1.000
		sol	−0.557	−0.564	−0.730	−0.760	−1.000
		Δ	−0.065	−0.057	−0.044	−0.074	0.000
	O	gas	−0.968	−1.016	−0.993	−0.949	−0.930
		sol	−0.985	−1.006	−0.991	−0.957	−0.934
		Δ	−0.017	0.010	0.002	−0.008	−0.004
	N	gas	−1.056	−1.049	−1.051	−1.028	−1.003
		sol	−1.038	−1.037	−1.032	−1.018	−0.999
		Δ	0.018	0.012	0.019	0.010	0.004
2	Pt	gas	0.612	0.626	0.772	0.760	0.794
		sol	0.642	0.645	0.781	0.772	0.793
		Δ	0.030	0.019	0.009	0.012	−0.001
	Cl	gas	−0.455	−0.494	−0.671	−0.581	−1.000
		sol	−0.540	−0.548	−0.705	−0.744	−1.000
		Δ	−0.085	−0.054	−0.034	−0.163	0.000
	O	gas	−0.968	−0.982	−1.013	−0.965	−0.956
		sol	−0.985	−0.984	−1.018	−0.962	−0.956
		Δ	−0.017	−0.002	−0.005	0.003	0.000
	N	gas	−1.063	−1.052	−1.041	−1.022	−1.003
		sol	−1.045	−1.038	−1.026	−1.013	−1.002
		Δ	0.018	0.014	0.015	0.009	0.001
3	Pt	gas	0.556	0.570	0.721	0.703	0.716
		sol	0.573	0.584	0.727	0.699	0.719
		Δ	0.017	0.014	0.006	−0.004	0.003
	Cl	gas	−0.473	−0.501	−0.697	−0.676	−1.000
		sol	−0.541	−0.549	−0.731	−0.769	−1.000
		Δ	−0.068	−0.048	−0.034	−0.093	0.000
	O	gas	−0.968	−1.015	−1.009	−0.969	−0.956
		sol	−0.985	−1.012	−1.011	−0.970	−0.956
		Δ	−0.017	0.003	−0.002	−0.001	0.000
	N	gas	−0.693	−0.685	−0.681	−0.667	−0.642
		sol	−0.678	−0.673	−0.668	−0.651	−0.643
		Δ	0.015	0.012	0.013	0.016	−0.001

[a] Phase gas and sol are gas phase and aqueous solution, respectively. Phase Δ is the solvent effect defined as the property in the aqueous solution minus that in gas phase.

computed and listed in Table 5. In line with the structural changes in the hydrolysis process, the most remarkable variations of atomic charges also occur in the four atoms which consist of the equatorial plane of the TBP-like structure. Among these four atoms, Pt and Cl have the largest charge variations, which is consistent with the largest bond length variation of R_{Pt-Cl}. Accordingly, the oxygen atom of the entering water molecule has a smaller charge change due to the smaller change of R_{Pt-O}, and the nitrogen atom of the ligand in the equatorial plane has the smallest charge change due to its smallest change of R_{Pt-N}. The similar tendencies of these charge changes can be seen in Figure 4 due to a common reaction mechanism. With the reaction proceeding, in contrast to the more positive atomic charge of the central platinum atom (Q_{Pt}), the atomic charge of the leaving ligand (Q_{Cl}) becomes more negative, indicating a charge transfer between these two groups. But the charge gain of the chlorine atom is greater than the charge loss of the platinum atom. To meet the charge conservation of the hydrolysis reaction, charge losses of other groups are required. The entering ligand, as illustrated by the oxygen atomic charge (Q_O), first increases its negative charge to favor the nucleophilic attack in the formation of a relatively stable I1 complex and then also releases some charges to the leaving ligand after TS. The resting ligand in the equator, though it has a minor contribution, continuously lends charges to the leaving ligand as reflected by the atomic charge of the equatorial nitrogen atom (Q_N). The total charge gains of the leaving ligand in the rate-determining step I1 → I2 are 0.196*e*, 0.196*e*, and 0.220*e*, respectively. In contrast, the total charge losses of the other three equatorial atoms are 0.172*e*, 0.174*e*, and 0.179*e*, respectively. Therefore, the charge-separating extent follows the order of $\Delta G_1 < \Delta G_2 \ll \Delta G_3$.

4. Solvent Effect on the Geometric and Energetic Properties Relevant to Hydrolysis Reactions of Cisplatin and Its Analogues. The above two sections discuss the geometric and energetic properties for title hydrolysis reactions in the aqueous solution for the sake of comparison with experiments performed on the same conditions. But most theoretical studies[2,7,18−21] of these transition metal complexes and their solution reactions were executed in the gas phase to reduce the computational cost. Such an effort to neglect the solvent effect may be justified in some cases where the solvent effect is not large or it does not alter the qualitative results among the series of complexes. Yet, for an accurate study of solution species and reactions, the solvent effect shall be included.

The solvent effect on structures of R, I1, TS, I2, and P were first examined here. It can be seen from Table 3 that the solvent effect of the M−L bond length (R_{Pt-Cl}) is greater than that of the M−E bond length (R_{Pt-O}), which is consistent with the relatively larger molecular volume of the leaving ligand (Cl^-) as 22.95 cm^3/mol than that of the entering ligand (H_2O) as 16.05 cm^3/mol based on the current mPW1PW91/SDD molecular volume calculations. The solvent effect makes R_{Pt-Cl} generally increase with the reaction proceeding R → I1 → TS → I2. R_{Pt-O} in each state of the three reactions is also amplified in general. At the same time, the L−M−E (∠Cl−Pt−O) bond angles were decreased in the aqueous solution. These structural modifications, which can lower the electronic repulsion imposed by the high steric effect in these complexes, further stabilized the solvated systems as evidenced by the decreased energies in Table S2 (Supporting Information). Each species in the studied reactions is stabilized by the aquation. The stabilization energies from the aquation are greater than 10 kcal/mol in the majority of these complexes, especially for reactions 1 and 2. The cyclic ligand environment of the dien complex in reaction 3, however, hinders the geometric modification required for the aquation so that the stabilization effect by the solvent is less than that in other two processes.

Comparing the solvent effects on all the structural parameters, it can be concluded that for the bond lengths, R_{Pt-Cl} and R_{Pt-O} were more affected than R_{Pt-N}, $R_{Pt-N'}$, and R_{Pt-X}, and for the bond angles, ∠Cl−Pt−O, ∠Cl−Pt−N, and ∠O−Pt−N were also more affected than ∠N−Pt−N′ and ∠N−Pt-X. This fact gives further evidence of the important role of the equatorial plane of the TBP-like structure in the hydrolysis process. In the stepwise reaction of the whole S_N2 procedure, the structural modifications imposed by the solvent reaction field become eminent in the rate-determining step I1 → TS → I2. As shown by the sum of three concentric angles in the equatorial plane, Σ, the solvent effect assists the equatorial four atoms N, Pt, O, and Cl to be coplanar in states I1, TS, and I2 for this key step reaction.

The overall solvent effects on the electronic property changes of each reaction were displayed in Table 4. It was usually not large for Δ*H* and Δ*G* of the whole process R → P as the solvent effect in each reaction was ∼6%. Yet, the difference of the solvent effect emerges in each rate-determining step reaction I1 → I2. Reaction 1 involves the formation of a (+1) and (−1)

(66) Reed, A. E.; Curtiss, L. A.; Weinhold, F. *Chem. Rev.* **1988**, *88*, 899.

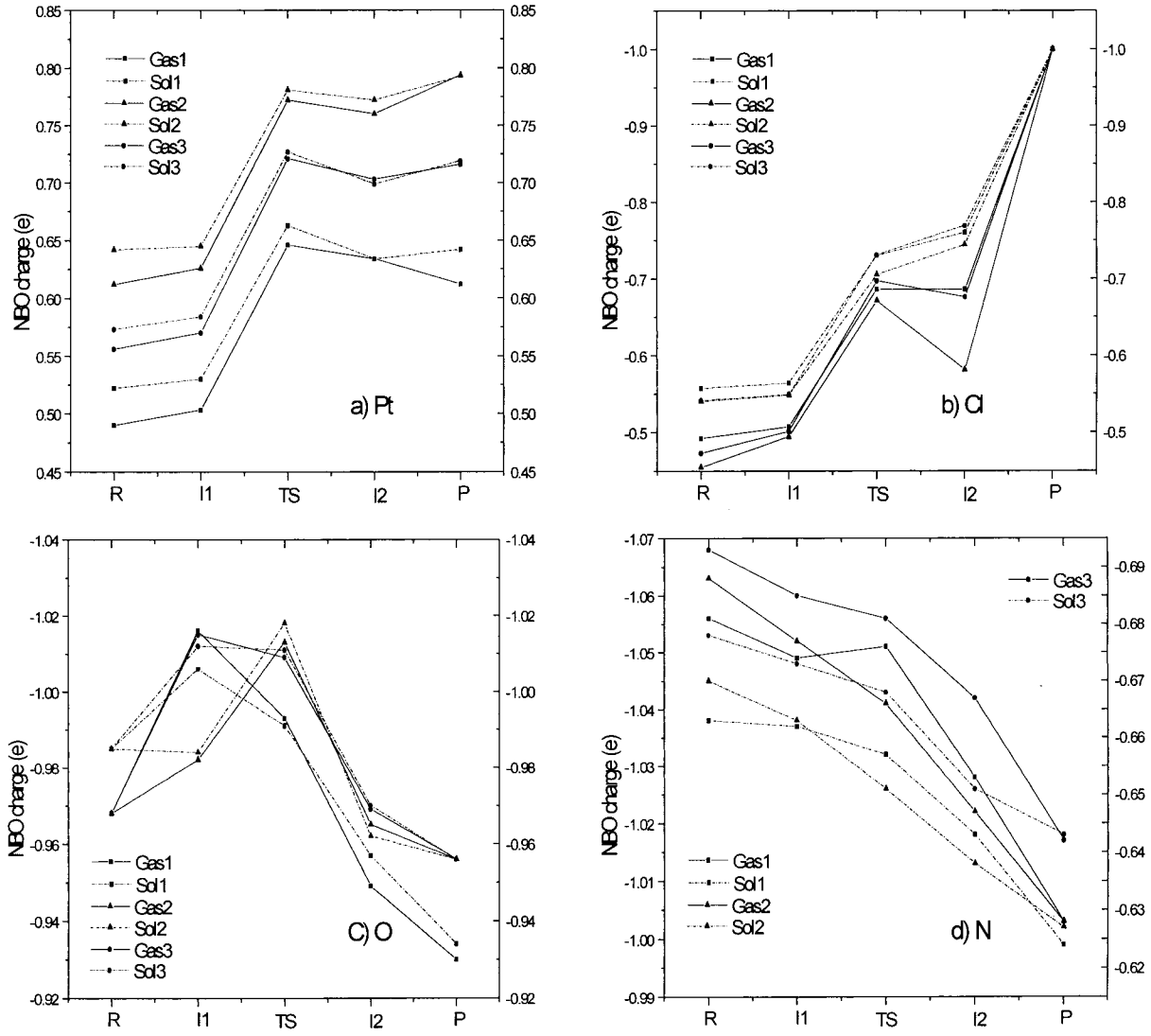

Figure 4. NBO charges of the four equatorial atoms, (a) Pt, (b) Cl, (c) O, and (d) N, in each model reaction. These states were connected by straight lines for clarity of the illustration. The symbols of Gas and Sol in this figure represent gas-phase reaction and aqueous solution reaction, respectively.

charged species from a neutral one, whereas reactions 2 and 3 involve the formation of a (+2) and (−1) charged species from a (+1) charged species. Although in theory there is an equal amount of charge separation in each reaction, the larger solvation effect would be expected in reactions 2 and 3 because the more charged system would take more solvation energy in the polar solvent (water here) to stabilize itself due to possible larger electrostatic interactions. Therefore, the smallest solvent effect occurs in reaction 1 as shown in Table 4. For the same reason, the solvation energies of I1, TS, and I2 in reactions 2 and 3 are in the same sequence as the charge separation extent in them (which becomes more as the hydrolysis proceeds further; see the previous NBO analysis), namely, I1 < TS < I2 as reflected in Table S2 (Supporting Information). In the relatively less charged species in reaction 1, the solvation energies are similar for I1, TS, and I2 (within 0.5 kcal/mol). Perhaps a more elaborate solvation model could reproduce more accurate quantitative results as regards their relative orders in this case. The less pronounced solvation effect in the key step of reaction 3 rather than reaction 2 can be accounted for by the relatively rigid cyclic ligand geometry in $[PtCl(dien)]^+$ compared to $[PtCl(OH_2)(NH_3)_2]^+$, where the stabilization imposed by the solvent reaction field is less effective in releasing structural strain in $[PtCl(dien)]^+$. As a matter of fact, it is the solvent effect that finally tunes the gas-phase results of ΔG in each I1 → I2 step to become compatible with the experimental outcomes of the studied hydrolysis reactions.

In accordance with the structural and energetic variations here, it is still the groups that play the most important roles in the hydrolysis processes that have the largest solvent effect of atomic charges, as clearly demonstrated by the equatorial four atoms' charges in Table 5 and Figure 4. The aquation makes the chief charge contributor—platinum—more positive and makes the charge collector—chlorine anion—more negative, which helps the charge-transfer process.

Conclusions

The prominent progress in computational transition metal chemistry has stimulated the current theoretical effort to obtain an accurate picture of the hydrolysis mechanisms of an important class of square-planar Pt(II) complexes, cisplatin and its analogues, using advanced computational methods on three typical reactions at the experimental temperature with the solvent effect included.

The true five stationary states in the second-order nucleophilic substitution pathway, namely, R → I1 → TS → I2 → P, in both gas phase and aqueous solution were obtained and characterized

theoretically for the first time for the hydrolysis reactions of title complexes. The five-coordinate TBP-like TS together with the five-coordinate intermediates have structures similar to those in other substitution reactions of square-planar transition metal complexes.[18,19] There was a clear correlation between the TS structures and hydrolysis behavior for title reactions; i.e., the reaction with a TS structure with smaller L−M−E angle and more lengthened M−L and M−E bonds will have a smaller Gibbs free energy change and accordingly the better hydrolysis yield (see Tables 3 and 4). The sum of L−M−E, L−M−R, and E−M−R bond angles in I1 and I2 are near 360°, while this value is almost 360° for TS in each reaction, indicating a coplanar position of N, Pt, O, and Cl in TS. Investigations of all structural changes in the hydrolysis process show that the most remarkable structural variations occur in the M−L and M−E bond lengths, and for the L−M−E, L−M−R, and E−M−R bond angles, suggesting the significant role of the equatorial plane of the TBP-like structure.

Consistent with the above aqueous geometric profiles, the aqueous energy profiles of the studied hydrolysis reactions apparently demonstrated a typical S_N2 shape of the reaction curve. The similar forward and backward $\Delta H^{\ddagger}$ and the correct change tendency of $\Delta S^{\ddagger}$ as in the experiments[15] were obtained in this work. In addition, the ΔG data of these three-step reactions are 3.72, 3.80, and 5.79 kcal/mol for hydrolysis reactions 1, 2, and 3, respectively, which conforms to the experimental fact[15,16] that $K_1 > K_2 \gg K_3$.

The NBO population analysis gave another picture of the title reactions. The crucial role of the equatorial plane can also be demonstrated by the fact that the most remarkable atomic charge variations in these reaction species occur in the four atoms which composes the equatorial plane of the TBP-like structure. The charge-separating extent follows the same order of $\Delta G_1 < \Delta G_2 \ll \Delta G_3$.

The solvent effect on title complexes and reactions were found to be critical in determining the structures, energies, and charges in most cases. The solvent effect generally increases the M−L and M−E bonds and decreases the L−M−E bond angle in the key step I1 → TS → I2, which can further reduce the electronic repulsion imposed by the high steric effect in these complexes to stabilize the solvated systems as evidenced by the decreased energies. Comparing the solvent effects on all the structural parameters, M−L and M−E bond lengths and L−M−E, L−M−R, and E−M−R bond angles of the equatorial plane of the TBP-like structure were among the most affected in the hydrolysis process. As shown by the sum of three concentric angles in the equatorial plane, $\sum$, the solvent effect assists the equatorial four atoms N, Pt, O, and Cl to be coplanar in states I1, TS, and I2 for this key step. On the basis of the current calculations, the solvent effect on title reactions cannot be neglected.

Taken together, the hydrolyses of cisplatin and its analogue undergo a common S_N2 reaction pathway where the equatorial plane of the five-coordinate TBP-like structure of the transition states and intermediates plays a significant role in determining the hydrolysis behavior. The solvent effect due to the important contribution to these aqueous reactions is considered to be essential for an accurate theory in this field. This work provides a thorough and detailed theoretical investigation on the mechanisms of hydrolyses of cisplatin and its analogues, which is likely to contribute to further understanding of the kinetics of the reaction of cisplatin with DNA and other biomolecules.

Acknowledgment. We are thankful for financial support from the Major State Basic Research Development Program (Grant G2000077500) of China, the University Key Teacher Fund from the Ministry of Education of China, the Distinguished Young Scientists Fund from the National Natural Science Foundation of China (Grant 29925102), State Key Project of the Fundamental Research, and Nanjing University Talent Development Foundation.

Supporting Information Available: Additional information as noted in text. This material is available free of charge at http://pubs.acs.org.

JA0023938